Transferable Graphene Oxide Films with Tunable Microstructures

Saad A. Hasan,[†,⊥] John L. Rigueur,[†] Robert R. Harl,[‡] Alex J. Krejci,[§] Isabel Gonzalo-Juan,[§] Bridget R. Rogers,[‡] and James H. Dickerson[§,*]

[†]Interdisciplinary Graduate Program in Materials Science, [‡]Department of Chemical and Biomolecular Engineering, and [§]Department of Physics and Astronomy, Vanderbilt University, Nashville, Tennessee 37235, United States. [⊥]Present address: Nanotechnology and Functional Materials, The Ångström Laboratory, Uppsala University, 751 21 Uppsala, Sweden.

ABSTRACT This report describes methods to produce large-area films of graphene oxide from aqueous suspensions using electrophoretic deposition. By selecting the appropriate suspension pH and deposition voltage, films of the negatively charged graphene oxide sheets can be produced with either a smooth "rug" microstructure on the anode or a porous "brick" microstructure on the cathode. Cathodic deposition occurs in the low pH suspension with the application of a relatively high voltage, which facilitates a gradual change in the colloids' charge from negative to positive as they adsorb protons released by the electrolysis of water. The shift in the colloids' charge also gives rise to the brick microstructure, as the concurrent decrease in electrostatic repulsion between graphene oxide sheets results in the formation of multilayered aggregates (the "bricks"). Measurements of water contact angle revealed the brick films (79°) to be more hydrophobic than the rug films (41°), a difference we attribute primarily to the distinct microstructures. Finally, we describe a sacrificial layer technique to make these graphene oxide films free-standing, which would enable them to be placed on arbitrary substrates.

KEYWORDS: graphene · electrophoretic deposition · free-standing · thin films · wetting

Colloidal graphenes[1−3] are immensely interesting to the scientific community, as the potential for large-scale production would facilitate their use in systems that harness their unique electrical and mechanical properties.[4,5] Challenges, inherent to the use of colloidal graphene to fabricate films and coatings, include control over the deposition site, the dimension of the films, and the arrangement of the graphene sheets within the deposit. Here, we report a straightforward method to produce centimeter-sized films of graphene oxide whose microstructure is controlled, in part, by tuning the pH of the aqueous suspension from which they are deposited. Different microstructures engender distinct surface wetting behaviors, as measured by water contact angle. We also demonstrate how the films can be made free-standing, which aids their transfer to arbitrary substrates. The techniques described here suggest one path by which graphene-based materials could be deployed rapidly into technologically significant coatings and devices.

Individual sheets of graphene with dimensions approaching 100 μm can be isolated from graphite by the "Scotch tape method" of mechanical cleavage,[6] allowing them to be placed on substrates and processed into electronic devices using lithographic methods.[7,8] However, mechanical cleavage is poorly suited for large-scale production of graphene. To increase the feasibility of graphene for electronic device applications, different groups have studied the growth of graphene layers *via* decomposition of silicon carbide.[9,10] As an alternative to "dry" techniques, the use of colloidal graphene has yielded an assortment of optoelectronic devices,[11,12] composite materials,[13−15] and functional coatings.[16] Suspension-based approaches are promising because the graphene can be prepared in large quantities and distributed rapidly onto nearly any surface.

Our approach utilizes aqueous dispersions of exfoliated graphene oxide (eGO) sheets, synthesized from powdered graphite using the modified Hummers method.[17,18] Individual sheets have a thickness of ~0.7 nm and lateral dimensions from 100 to 1000 nm (Figure 1a). The suspension of eGO sheets is obtained by sonication of graphite oxide in deionized water (see Methods). Oxygen-containing groups, like epoxides and carboxylic acids, contribute to the hydrophilic character of eGO, aiding the formation of aqueous suspensions. When suspended in water, carboxylic acid groups, present on the edges of the sheets,[19] are deprotonated to yield negatively charged moieties. Measurement of the electrophoretic mobility (μ) of the sheets reveals information about their

*Address correspondence to james.h.dickerson@vanderbilt.edu.

Received for review August 25, 2010 and accepted November 11, 2010.

Published online November 29, 2010. 10.1021/nn102152x

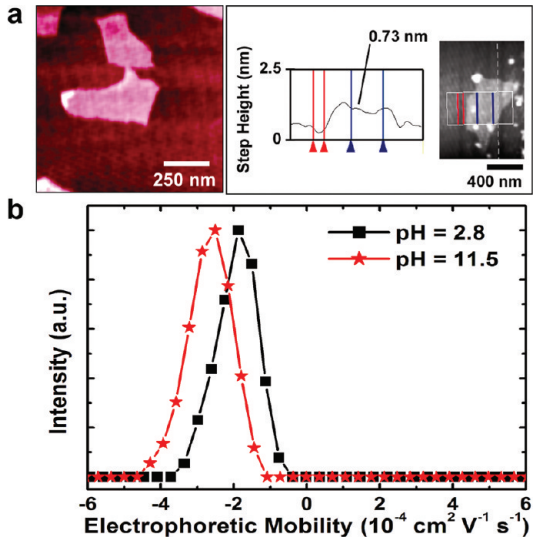

Figure 1. Exfoliated graphene oxide (eGO) sheets. (a) An individual eGO sheet, imaged using atomic force microscopy, with a thickness of ~0.7 nm. (b) Electrophoretic mobility of eGO sheets in aqueous suspensions with pH values of 11.5 and 2.8. The absolute value of the electrophoretic mobility of the acidic suspension is lower because the abundant protons in the suspension can neutralize some of the negatively charged groups on the sheets.

charge state.[20] In both of the reported pH conditions (pH = 2.8 and 11.5), the eGO sheets have a net negative charge (Figure 1b). Electrostatic repulsion among the negative charges stabilizes the suspension of eGO sheets by preventing their aggregation due to van der Waals forces, per the Derjaguin–Landau–Verwey–Overbeek (DLVO) theory.[21] These charges also facilitate the assembly of the eGO sheets *via* electrophoretic deposition (EPD).

In EPD, an applied electric field drives charged particles toward a field-emanating surface. Under the proper conditions, particles aggregate to form a layered deposit that adheres to the surface.[22] The formation of a homogeneous, closely packed deposit requires the use of a stable suspension in which the particles are dispersed with minimal aggregation.[23] Stable suspensions of a wide assortment of materials can be prepared by tuning the particle–particle interactions,[24] foremost of which are attractive van der Waals forces and repulsive electrostatic forces. EPD offers several advantages over other colloidal processing techniques, including enhanced deposition rate, long-range morphological uniformity in the deposit, site-selectivity, and size-scalability among others.[25–28] Because of these advantages, EPD has been the focus of wide-ranging study in academic and industrial settings, especially for the manufacture of ceramic materials.[25,29,30] Additionally, the morphology of electrophoretically formed deposits may be tuned by performing the deposition in the presence of external mediating forces such as a magnetic field.[31,32]

The technique of EPD continues to be of interest for new materials such as graphene. EPD can deposit multiple layers of colloidal graphene and may improve the conductivity of previously oxidized graphene through reduction electrochemistry.[12,33,34] In this report, we show how multilayered films can be formed with concurrent tuning of the morphology and the physical properties of the graphene deposits using EPD alone, with no external mediating forces.

RESULTS AND DISCUSSION

By using eGO suspensions with different pH values, we fabricated multilayered films with different microstructures. In all experiments, dc voltages were applied between parallel electrodes placed in the suspensions with a separation of 5 mm (see Methods). In the absence of applied voltage, no visible film formed on either electrode. Figure 2 panels a–c show a film of eGO deposited onto stainless steel from a suspension with a pH of 11.5 (designated "susp-A") using 3 V for 10 min. Negatively charged eGO sheets deposited on the anode, whereas nothing deposited on the cathode. Using these conditions, films deposited over the entirety of the electrode that was submerged in the liquid. From scanning electron microscopy (SEM), the outlines of overlapping eGO sheets were visible. Apart from intermittent wrinkles, the sheets appeared to lie flat and parallel to the electrode surface, an orientation observed in previous EPD studies using colloidal graphene and other powders with a high aspect ratio.[33–35] We designated these films to have a "rug" microstructure to reflect the flat-but-occasionally wrinkled topology of the eGO sheets that evoked the image of a throw rug.

Figure 2 panels d–f show a film of eGO deposited onto stainless steel from a suspension with pH of 2.8 (designated "susp-B") using 15 V for 10 min. Although these eGO sheets also were negatively charged, the resulting films remarkably formed on the cathode. The anode showed only micrometer-sized regions of deposited eGO after the EPD experiment (see Supporting Information). The films, which deposited on the cathode using these conditions, exhibited nearly complete coverage of the area that was submerged in the liquid. The films comprised microscale domains of flat eGO sheets; these domains appeared to be stacked with different heights. Interspersed among these domains were voids of area $\leq 10\ \mu m^2$. This microstructure suggested that the eGO sheets formed face-to-face adhering multilayers prior to depositing on the electrode. We designated these films to have a "brick" microstructure to reflect the face-to-face adhering multilayers, or bricks, that formed domains in unevenly deposited casts in an otherwise continuous, yet porous film. Complementary imaging of the films using atomic force microscopy (AFM) corroborated the microstructures determined by SEM (see Supporting Information).

Measurement of the surface wettability of the eGO films revealed that films with brick microstructure were more hydrophobic than films with rug microstructure

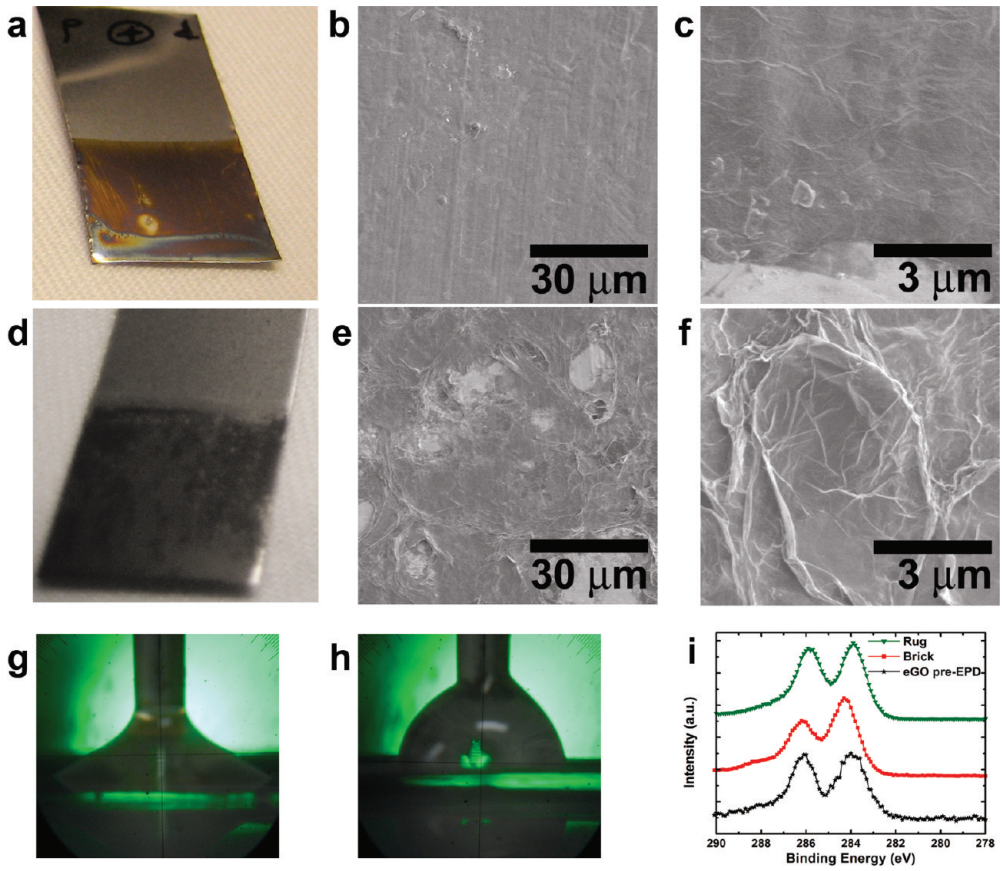

Figure 2. Characterization of electrophoretically deposited eGO films. Films with rug microstructure shown in a photograph (a) and in SEM images (b,c). Films with brick microstructure shown in a photograph (d) and in SEM images (e,f). Water contact angles for the rug (g) and brick (h) films, 41° and 79°, respectively. (i) XPS measurements of the C 1s spectra for the rug and brick eGO films and the eGO sheets prior to EPD. Since the C 1s spectra remain largely unchanged after EPD, we subsequently attributed the associated higher contact angle of the brick films to microscale voids, such as air pockets, not to film chemistry. This is supported by the Cassie−Baxter model, which considers the film's surface as a composite of eGO and air. With air, water is assigned a contact angle of 180°.

(Figure 2g,h). The notably dissimilar contact angles, 41° ± 2° for rug films *versus* 79° ± 4° for brick films, can be attributed to primarily microstructure differences. The Cassie−Baxter model[36] of surface wetting predicts that films become more hydrophobic with increasing roughness since a growing fraction of the surface comprises pockets of air, whose contact angle is 180°. Thus, we inferred that voids in the brick micro-

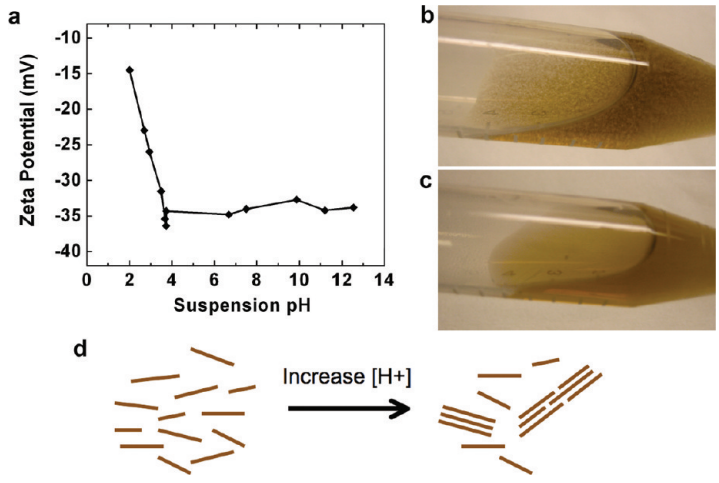

Figure 3. Understanding eGO suspension properties as a function of suspension pH. (a) Zeta potential of the eGO sheets as a function of suspension pH (measurement error: pH, ±0.1; zeta potential, ±1 mV); (b) suspension with zeta potential −15 mV exhibiting the formation of flocculants; (c) suspension with zeta potential −35 mV free of aggregates; (d) schematic indicating the manner in which eGO sheets form aggregates as the suspension pH decreases.

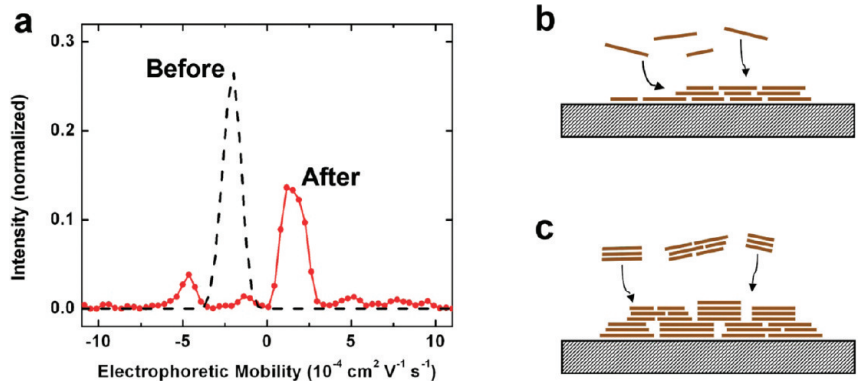

Figure 4. Microstructure arising due to modification of colloidal charge. (a) Electrophoretic mobility measurements of susp-B before and after performing EPD, indicating that the charge on the eGO sheets has reversed from negative to positive. Schematics showing how individual eGO sheets give rise to the rug microstructure (b) while the formation of stacked-sheet aggregates gives rise to the brick microstructure (c).

structure increased the contact angle of the otherwise hydrophilic eGO film.

X-ray photoelectron spectroscopy (XPS) measurements characterized the chemical composition of the films (see Supporting Information). Figure 2i shows the C 1s spectra for both films and for the eGO prior to EPD; all of the spectra show peaks for C−C, C−O, and C═O bonding, suggesting that the colloidal building block is largely unchanged after the EPD process. The weaker C−O bonding signal relative to the C−C bonding signal in the brick eGO film may be evidence of some electrochemical reduction during the deposition process, similar to previous observations.[34] The decrease in C−O content alone, however, is not sufficient to explain the different contact angles, as many of the hydrophilic carboxylic acid groups remained in the brick film.

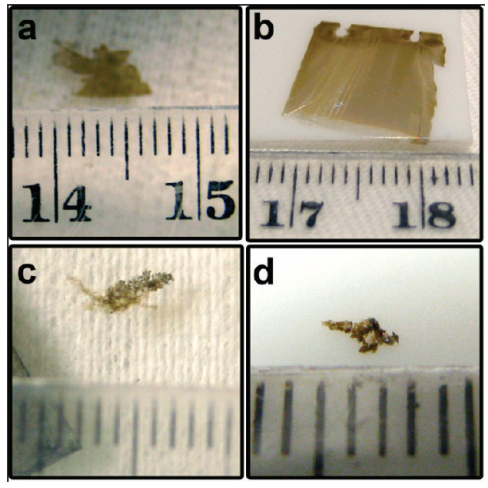

Figure 5. Transferable eGO films. Steel substrates coated with cellulose acetate were used as a sacrificial polymer layer upon which eGO films were cast. Unlike the previously reported sacrificial layer EPD technique, the deposited eGO films required some encouragement to liberate from the underlying substrate. Films with rug microstructure floating on the meniscus of the acetone bath after liberation from the steel substrate (a) and transferred to a Teflon sheet (b). Similarly, films with brick microstructure floating on the meniscus of the acetone bath (c) and transferred to a Teflon sheet (d). The ruler shown in all four frames is demarcated in millimeters.

The electrolysis of water is central to the mechanism of eGO deposition for both suspensions. At the anode, water decomposed to yield oxygen gas and dissolved protons, while electrons from the cathode combined with protons to form hydrogen gas. These gases were observed as bubbles evolving from the electrode surfaces. To investigate the effect of partially dissolved protons on the eGO suspensions, we measured the zeta potential (ζ) of the colloids at different pH values. ζ is associated with the degree of colloidal stability; typically, 30 mV is the threshold above which colloids are considered stable and are not prone to aggregation.[21] For the probed pH values, ζ ranged from -15 to -35 mV (Figure 3a). Stable suspensions were achieved at pH $\geq$ 3.6, whereas suspensions with a pH of $\sim$2.0 ($\zeta = -15$ mV) exhibited flocculation (Figure 3b). In contrast, the suspensions used in our experiments (susp-A, $\zeta = -35.0$ mV; susp-B, $\zeta = -25.7$ mV) remained free of flocculation or settling for durations ranging from 24 h for susp-B to indefinitely for susp-A (Figure 3c). Thus, a proton concentration increase can trigger aggregation of the eGO sheets, resulting from charge screening on the sheets that attenuates their electrostatic repulsion between them. The shape of the eGO sheets favors their aggregation by face-to-face stacking rather than edge-to-edge or edge-to-face adhesion[37] (Figure 3d).

During EPD from susp-A, the increase in proton concentration at the anode due to water electrolysis decreased the electrostatic repulsion between eGO sheets, enabling them to deposit on the anode. In susp-B, the deposition of eGO sheets on the cathode indicated a charge reversal from negative to positive that occurred during the experiment. Measurements of μ of the suspension before and after EPD verified the transition to positively charged colloids (Figure 4a). This, the charge of the colloids shifted from $\zeta = -25.7$ mV toward more positive values with the generation of protons. In Figure 3b, the eGO sheets began aggregating at -15 mV. This aggregation would have continued as ζ approached 0 mV as the electrostatic repulsion be-

tween sheets decreased further. Once the aggregates of multilayered eGO sheets formed, strong van der Waals attraction between the sheets prevented them from being readily separated. Thus, the aggregate formation and associated charge reversal during EPD from susp-B explain the film's brick microstructure (Figure 4c). This phenomenon of charge reversal for EPD using 15 V in susp-B was evident in deposition runs shorter than 10 min, as well. When the deposition time was 5 min, a film similar to that in Figure 2d was formed on the cathode over the entire submerged area; this film appeared less filled-in due to the shorter deposition time (see Supporting Information).

To broaden the potential of using eGO films in varied applications, we investigated using EPD in combination with a sacrificial layer technique, which would produce free-standing eGO films. Sacrificial layer electrophoretic deposition was demonstrated previously with nanocrystals using an insulating polymer that dissolved in water.[38] Since our eGO suspensions contain water, we cast onto our substrates cellulose acetate, which is hydrophilic but insoluble in water.[39] After depositing eGO atop cellulose acetate, we submerged the substrates in acetone to liberate the films. After the polymer had dissolved, we guided a razor parallel to the steel surface underneath the film to remove the film from the solvent.[40] This procedure yielded macroscopic eGO films from both susp-A (Figure 5a,b) and susp-B (Figure 5c,d), which were transferable to arbitrary locations.

In conclusion, we have used EPD to produce large-area films of colloidal graphene while controlling the site of the deposition and the microstructure of the deposited films. The films' microstructures yielded distinct surface wetting characteristics, which may have technological implications in functional coating applications. The capability of making free-standing films may result in the deployment of these flexible, high-surface-area films in display screens and energy storage devices. The use of EPD may facilitate their integration in large-scale manufacturing when combined with rapid techniques like roll-to-roll production.

METHODS

Formation of Exfoliated Graphene Oxide (eGO). Graphite oxide was synthesized from powdered graphite using the modified Hummers method.[17,18] Bay Carbon, Inc. provided a sample of graphite (catalog item SP-1). All other reagents were purchased from Sigma-Aldrich. After the synthesis, the graphite oxide was washed with dilute HCl and deionized water on a filter and then freeze-dried to enable accurate measurements of the powder mass. For the EPD experiments and suspension characterization, suspensions of eGO were prepared at a concentration of 0.35 mg/mL. Their pH was tuned using HCl and KOH. In the EPD runs, the electrodes, typically of 316 L stainless steel (McMaster Carr), were mounted parallel to each other with separation of 5 mm. The dc voltage was applied before dipping the electrodes into the eGO suspension and remained on for 5 min after the electrodes were withdrawn from the suspension.

Microscopic Characterization. The dimensions of individual eGO sheets were examined by atomic force microscopy (AFM). Samples for AFM were prepared by spin-casting the eGO suspension over a freshly cleaved mica surface at 4000 rpm for 60 s. AFM imaging was done with a Digital Instruments Nanoscope III operating in tapping mode. The electrophoretic mobility of the eGO suspensions was measured using a Malvern Instruments Zetasizer Nano ZS. Zeta potentials were calculated from the measured mobility using the Smoluchowski approximation. The microstructure of the eGO films was probed using a Hitachi S-4200 scanning electron microscope operating at 1 kV. Water contact angles were measured using a Ramé-Hart contact angle goniometer. Contact angles reported here are the advancing contact angles. XPS measurements were performed in an Ulvac-PHI 5000 VersaProbe spectrometer using a monochromatic Al Kα x-ray beam (1486.6 eV). A 25 W, 100 μm spot size was used in all data acquisition with both 1.1 eV electron and 10 eV Ar ion neutralization. Photoelectrons were collected at 45° to the sample normal into a spherical capacitor analyzer. Survey scans were acquired for the range 0−1300 eV using a pass energy of 187.85 eV. High-resolution scans for C 1s bonding were acquired using a pass energy of 23.5 eV. Data analysis and peak fitting were done with the CasaXPS software package.

Formation of Freestanding eGO Films. The freestanding eGO films were prepared by modifying the sacrificial layer technique reported previously.[38] A 110 nm layer of cellulose acetate (M_W = 30 000, Sigma-Aldrich) was spun cast onto the electrodes at 1000 rpm for 60 s from a 10 mg/mL solution in acetone. After deposition of the eGO films, the electrodes were soaked overnight in acetone to dissolve the cellulose acetate. A single-edge razor blade was pushed along the film−substrate interface to complete the liberation of the films.[40]

Acknowledgment. The authors acknowledge Steven Vilt for assistance with contact angle measurements, Dr. Tony Hmelo for access to the spin-caster, Andrés Delannoy for photographing one of the films, and Line Everlund Matulac for assistance preparing the table of contents graphic. This work was supported by the Vanderbilt Discovery Grant and NSF-CBET-0723077.

Supporting Information Available: Synthesis of graphite oxide and preparation of eGO suspensions; EPD parameters; electrode photographs; description of characterization by AFM, zetasizer, SEM, and XPS; parameters for sacrificial layer electrophoretic deposition; survey scans from XPS measurements. This material is available free of charge *via* the Internet at http://pubs.acs.org.

REFERENCES AND NOTES

1. Park, S.; Ruoff, R. S. Chemical Methods for the Production of Graphenes. *Nat. Nanotechnol.* **2009**, *4*, 217–224.
2. Li, D.; Muller, M. B.; Gilje, S.; Kaner, R. B.; Wallace, G. G. Processable Aqueous Dispersions of Graphene Nanosheets. *Nat. Nanotechnol.* **2008**, *3*, 101–105.
3. Tung, V. C.; Allen, M. J.; Yang, Y.; Kaner, R. B. High-Throughput Solution Processing of Large-Scale Graphene. *Nat. Nanotechnol.* **2009**, *4*, 25–29.
4. Novoselov, K. S.; Geim, A. K.; Morozov, S. V.; Jiang, D.; Katsnelson, M. I.; Grigorieva, I. V.; Dubonos, S. V.; Firsov, A. A. Two-Dimensional Gas of Massless Dirac Fermions in Graphene. *Nature* **2005**, *438*, 197–200.
5. Lee, C.; Wei, X. D.; Kysar, J. W.; Hone, J. Measurement of the Elastic Properties and Intrinsic Strength of Monolayer Graphene. *Science* **2008**, *321*, 385–388.
6. Novoselov, K. S.; Geim, A. K.; Morozov, S. V.; Jiang, D.; Zhang, Y.; Dubonos, S. V.; Grigorieva, I. V.; Firsov, A. A. Electric Field Effect in Atomically Thin Carbon Films. *Science* **2004**, *306*, 666–669.
7. Schedin, F.; Geim, A. K.; Morozov, S. V.; Hill, E. W.; Blake, P.;

Katsnelson, M. I.; Novoselov, K. S. Detection of Individual Gas Molecules Adsorbed on Graphene. *Nat. Mater.* **2007**, *6*, 652–655.
8. Chen, C. Y.; Rosenblatt, S.; Bolotin, K. I.; Kalb, W.; Kim, P.; Kymissis, I.; Stormer, H. L.; Heinz, T. F.; Hone, J. Performance of Monolayer Graphene Nanomechanical Resonators with Electrical Readout. *Nat. Nanotechnol.* **2009**, *4*, 861–867.
9. Berger, C.; Song, Z. M.; Li, T. B.; Li, X. B.; Ogbazghi, A. Y.; Feng, R.; Dai, Z. T.; Marchenkov, A. N.; Conrad, E. H. Ultrathin Epitaxial Graphite: 2D Electron Gas Properties and a Route toward Graphene-Based Nanoelectronics. *J. Phys. Chem. B* **2004**, *108*, 19912–19916.
10. Emtsev, K. V.; Bostwick, A.; Horn, K.; Jobst, J.; Kellogg, G. L.; Ley, L.; McChesney, J. L.; Ohta, T.; Reshanov, S. A. Towards Wafer-Size Graphene Layers by Atmospheric Pressure Graphitization of Silicon Carbide. *Nat. Mater.* **2009**, *8*, 203–207.
11. Eda, G.; Fanchini, G.; Chhowalla, M. Large-Area Ultrathin Films of Reduced Graphene Oxide as a Transparent and Flexible Electronic Material. *Nat. Nanotechnol.* **2008**, *3*, 270–274.
12. Wu, Z. S.; Pei, S.; Ren, W. C.; Tang, D. M.; Gao, L. B.; Liu, B. L.; Li, F.; Liu, C.; Cheng, H. M. Field Emission of Single-Layer Graphene Films Prepared by Electrophoretic Deposition. *Adv. Mater.* **2009**, *21*, 1–5.
13. Stankovich, S.; Dikin, D. A.; Dommett, G. H. B.; Kohlhaas, K. M.; Zimney, E. J.; Stach, E. A.; Piner, R. D.; Nguyen, S. T.; Ruoff, R. S. Graphene-Based Composite Materials. *Nature* **2006**, *442*, 282–286.
14. Rafiee, M. A.; Rafiee, J.; Wang, Z.; Song, H. H.; Yu, Z. Z.; Koratkar, N. Enhanced Mechanical Properties of Nanocomposites at Low Graphene Content. *ACS Nano* **2009**, *3*, 3884–3890.
15. Kulkarni, D. D.; Choi, I.; Singamaneni, S. S.; Tsukruk, V. V. Graphene Oxide−Polyelectrolyte Nanomembranes. *ACS Nano* **2010**, *4*, 4667–76.
16. Rafiee, J.; Rafiee, M. A.; Yu, Z. Z.; Koratkar, N. Superhydrophobic to Superhydrophilic Wetting Control in Graphene Films. *Adv. Mater.* **2010**, *22*, 2151–2154.
17. Hummers, W. S.; Offeman, R. E. Preparation of Graphitic Oxide. *J. Am. Chem. Soc.* **1958**, *80*, 1339.
18. Park, S.; An, J. H.; Piner, R. D.; Jung, I.; Yang, D. X.; Velamakanni, A.; Nguyen, S. T.; Ruoff, R. S. Aqueous Suspension and Characterization of Chemically Modified Graphene Sheets. *Chem. Mater.* **2008**, *20*, 6592–6594.
19. Lerf, A.; He, H. Y.; Forster, M.; Klinowski, J. Structure of Graphite Oxide Revisited. *J. Phys. Chem. B* **1998**, *102*, 4477–4482.
20. Shevchenko, E. V.; Talapin, D. V.; Kotov, N. A.; O'Brien, S.; Murray, C. B. Structural Diversity in Binary Nanoparticle Superlattices. *Nature* **2006**, *439*, 55–59.
21. Hunter, R. J. *Foundations of Colloid Science*; 2nd ed.; Oxford University Press: Oxford; New York, 2001; p xii, 806.
22. Hamaker, H. C. Formation of a Deposit by Electrophoresis. *Trans. Faraday Soc.* **1940**, *35*, 0279−0286.
23. Sarkar, P.; De, D.; Rho, H. Synthesis and Microstructural Manipulation of Ceramics by Electrophoretic Deposition. *J. Mater. Sci.* **2004**, *39*, 819–823.
24. Hamaker, H. C.; Verwey, E. J. W. (C) Colloid Stability. The Role of the Forces between the Particles in Electrodeposition and Other Phenomena. *Trans. Faraday Soc.* **1940**, *35*, 0180−0185.
25. Van der Biest, O. O.; Vandeperre, L. J. Electrophoretic Deposition of Materials. *Annu. Rev. Mater. Sci.* **1999**, *29*, 327–352.
26. Boccaccini, A. R.; Roether, J. A.; Thomas, B. J. C.; Shaffer, M. S. P.; Chavez, E.; Stoll, E.; Minay, E. J. The Electrophoretic Deposition of Inorganic Nanoscaled Materials. *J. Ceram. Soc. Jpn.* **2006**, *114*, 1–14.
27. Maenosono, S.; Okubo, T.; Yamaguchi, Y. Overview of Nanoparticle Array Formation by Wet Coating. *J. Nanopart. Res.* **2003**, *5*, 5–15.
28. Mahajan, S. V.; Dickerson, J. H. Understanding the Growth of Eu_2O_3 Nanocrystal Films Made *via* Electrophoretic Deposition. *Nanotechnology* **2010**, *21*, 145704.
29. Sarkar, P.; Nicholson, P. S. Electrophoretic Deposition (EPD): Mechanisms, Kinetics, and Application to Ceramics. *J. Am. Ceram. Soc.* **1996**, *79*, 1987–2002.
30. Verde, M.; Caballero, A. C.; Iglesias, Y.; Villegas, M.; Ferrari, B. Electrophoretic Deposition of Flake-Shaped ZnO Nanoparticles. *J. Electrochem. Soc.* **2010**, *157*, H55–H59.
31. Hein, M.; Muller, G.; Piel, H.; Ponto, L.; Becks, M.; Klein, U.; Peiniger, M. Electrophoretic Deposition of Textured $YBa_2Cu_3O_7-X$ Films on Silver Substrates. *J. Appl. Phys.* **1989**, *66*, 5940–5943.
32. Uchikoshi, T.; Suzuki, T. S.; Sakka, Y. Crystalline Orientation of Alumina Ceramics Prepared by Electrophoretic Deposition under a High Magnetic Field. *J. Mater. Sci.* **2006**, *41*, 8074–8078.
33. Lee, V.; Whittaker, L.; Jaye, C.; Baroudi, K. M.; Fischer, D. A.; Banerjee, S. Large-Area Chemically Modified Graphene Films: Electrophoretic Deposition and Characterization by Soft X-ray Absorption Spectroscopy. *Chem. Mater.* **2009**, *21*, 3905–3916.
34. An, S. J.; Zhu, Y. W.; Lee, S. H.; Stoller, M. D.; Emilsson, T.; Park, S.; Velamakanni, A.; An, J. H.; Ruoff, R. S. Thin Film Fabrication and Simultaneous Anodic Reduction of Deposited Graphene Oxide Platelets by Electrophoretic Deposition. *J. Phys. Chem. Lett.* **2010**, *1*, 1259–1263.
35. Sarkar, P.; Mathur, S.; Nicholson, P. S.; Stager, C. V. Fabrication of Textured Bi−Sr−Ca−Cu−O Thick-Film by Electrophoretic Deposition. *J. Appl. Phys.* **1991**, *69*, 1775–1777.
36. Cassie, A. B. D.; Baxter, S. Wettability of Porous Surfaces. *Trans. Faraday Soc.* **1944**, *40*, 0546−0550.
37. Cote, L. J.; Kim, F.; Huang, J. X. Langmuir−Blodgett Assembly of Graphite Oxide Single Layers. *J. Am. Chem. Soc.* **2009**, *131*, 1043–1049.
38. Hasan, S. A.; Kavich, D. W.; Dickerson, J. H. Sacrificial Layer Electrophoretic Deposition of Free-Standing Multilayered Nanoparticle Films. *Chem. Commun.* **2009**, 3723–3725.
39. Mamedov, A. A.; Kotov, N. A. Free-Standing Layer-by-Layer Assembled Films of Magnetite Nanoparticles. *Langmuir* **2000**, *16*, 5530–5533.
40. Rigueur, J. L.; Hasan, S. A.; Mahajan, S. V.; Dickerson, J. H. Buckypaper Fabrication by Liberation of Electrophoretically Deposited Carbon Nanotubes. *Carbon* **2010**, *48*, 4090–4099.